



HAL
open science

A method to take account of the geometrical imperfections of quasi-spherical indenters

Philippe Brammer, Xavier Hernot, Gerard Mauvoisin, Olivier Bartier,
Simon-Serge Sablin

► **To cite this version:**

Philippe Brammer, Xavier Hernot, Gerard Mauvoisin, Olivier Bartier, Simon-Serge Sablin. A method to take account of the geometrical imperfections of quasi-spherical indenters. *Materials & Design*, 2013, 49, pp.406-413. 10.1016/j.matdes.2013.01.028 . hal-00861049

HAL Id: hal-00861049

<https://univ-rennes.hal.science/hal-00861049>

Submitted on 12 Sep 2013

HAL is a multi-disciplinary open access archive for the deposit and dissemination of scientific research documents, whether they are published or not. The documents may come from teaching and research institutions in France or abroad, or from public or private research centers.

L'archive ouverte pluridisciplinaire **HAL**, est destinée au dépôt et à la diffusion de documents scientifiques de niveau recherche, publiés ou non, émanant des établissements d'enseignement et de recherche français ou étrangers, des laboratoires publics ou privés.

A method to take account of the geometrical imperfections of quasi-spherical indenters

P. Brammer^{1,2}, X.Hernot¹, G. Mauvoisin¹, O. Bartier¹ and S.-S. Sablin²

¹LGCGM, 20 Avenue des Buttes de Coësmes, 35708 Rennes Cedex, France

²Technocentre Renault, Engineering Cost Control Department, 1 avenue du Golf, 78288

Guyancourt Cedex, France

**Corresponding author: philippe.brammer@univ-rennes1.fr*

(+33)6.32.66.29.74

Abstract

Perfect indenter geometry is quite difficult to manufacture, especially in the nano and macro scales. Indentation curves obtained with imperfect indenter geometry can show strong differences with those obtained with assumed perfect indenter geometry, thereby leading to erroneous data exploitation results.

This numerical study brings out the effect of imperfect spherical indenter geometry on indentation load-penetration depth curves, and on the mechanical properties identified by a reverse analysis model based on ideal spherical geometry. It is shown that a method to take account of geometrical imperfections is essential. Two correction methods based on geometrical and physical considerations are assessed, as well as the relevance of the use of the penetration data or the contact data. A method based on the equality of mean contact pressures and indenter volumes under the contact surface is found to be most relevant, as confirmed by the quality results obtained after application of a reverse analysis model.

The proposed method is of particular interest in the case of the use of an imperfect indenter whose profile is accurately known.

Keywords

Instrumented indentation; geometrical imperfection; reverse analysis; stress-strain curve

1. Introduction

The instrumented indentation test allows for an evaluation of mechanical properties of materials at macro, micro, and nano scales. The major assets of this test are its easy application at small scales and its quasi non destructive aspect. The indentation data, or indentation curve, is obtained by continuously measuring the applied load F and penetration depth h of a stiff indenter of known geometry normally to the surface of the tested sample. **Fig. 1** shows the geometric values of interest during the indentation by an indenter of arbitrary axisymmetric shape, in the case of the creation of either pile-up (**Fig. 1(a)**) or sink-in (**Fig. 1(b)**) at the surface of the sample. These values are referred to as the penetration depth h , the contact depth h_c , the surface contact radius a , and the contact radius a_c .

(a) (b)

Fig. 1. Geometric values of interest in the cases of (a) pile-up and (b) sink-in

Early data analysis methods [1-3] were aimed at evaluating elastic modulus and hardness without the observation of a residual imprint which is required by standard hardness tests. These methods are described by the international standards on instrumented indentation [4-7]. Methods were also proposed to evaluate flow properties of materials [8-21]. These methods, for which no standards are available, are either based on a representative stress-strain approach and require the evaluation or measurement of the contact radius a_c at discrete points [8, 9], or on reverse analysis models which only require the $F-h$ data [10-21].

Most data analysis methods are based on ideal indenter geometry. However, perfect geometry is quite difficult to achieve at low scales, therefore inducing major errors when analysing instrumented indentation data.

In the case of sharp indenters, which are widely used for the evaluation of elastic modulus and hardness due to their geometrical self-similarity, Oliver and Pharr [1] suggested a since widely-used area function to take account of indenter bluntness in the case of a Berkovitch 3-sided pyramid, expressed by Eq. (1).

$$A_c = 24.5h_c^2 + \sum_{i=1}^8 C_i h_c^{2(i-1)} \quad (1)$$

with A_c the contact area, 24.5 the proportionality factor between A_c and the square of h_c in the case of an ideal Berkovitch indenter and C_i the additional factors which represent the bluntness of the indenter tip.

In the case of spherical indenters, which are very convenient for the evaluation of flow properties because they induce penetration depth-dependent stress-strain fields, the analysis of the indentation data is subject to a length scale, i.e. the indenter radius, and the data analysis methods do not rely on an area function. Research studies [22-24] on the calibration of the geometrical imperfections of spherical indenters used the profiling of the residual imprint by Atomic Force Microscopy to define an effective indenter radius R_{eff} as expressed by Eq. (2).

$$R_{eff} = \frac{a_c^2 + h_c^2}{2h_c} \quad (2)$$

The use of this effective radius significantly improved the results obtained by a representative stress-strain based method [23, 24]. In the case of a reverse analysis model, Collin et al. [17, 18, 25] proposed an equivalent radius R_{eq} to correct the indentation curve obtained with a non spherical indenter. However, this relation was obtained by fitting of numerical data and is only relevant for a particular indenter.

The present work aims at an increased understanding of which geometrical and physical quantities allow for the transformation of an indentation curve obtained with an imperfect spherical indenter into an indentation curve which would be obtained with an ideal spherical indenter. The main objective of this transformation is to allow the application of reverse analysis models based on ideal spherical geometry to indentation data obtained with imperfect indenter geometry. In section 2, the effect of imperfect indenter geometry on numerical indentation curves obtained on twelve materials is brought out. In section 3, two geometrical correction methods are assessed as well as the relevance of the use of the penetration data or the contact data. In section 4, a reverse analysis model based on ideal spherical geometry is applied to ideal, initial, and corrected data to confirm the relevance of the proposed correction method.

2. Numerical highlight of the effect of indenter geometry on the indentation curve

The geometry of an actual axisymmetric rounded tip carved in bulk tungsten carbide of nominal radius 0.25 mm is used. This indenter was used in some of the authors' previous work [26]. The profile of this indenter was measured by Scanning Electronic Microscopy (SEM). Furthermore, in order to assess its smoothness, the profile was fitted by a sum of three power law functions as expressed by Eq. (3).

$$r(z) = \sum_{i=1}^3 \alpha_i z^{\beta_i} \quad (3)$$

The measured profile is compared to the fitted profile and to a spherical profile of radius $R'=0.25$ mm in **Fig. 2(a)**, and the difference between the fitted profile and the measured profile is shown in **Fig. 2(b)**.

(a) **(b)**

Fig. 2. (a) Measured indenter profile (Scanning Electronic Microscopy) and **(b)** difference between the fitted and the measured profile

The overall profile of the indenter is very different from a spherical profile of radius $R'=0.25$ mm, as can be observed in **Fig. 2(a)**. Furthermore, the profile shows irregularities which are shown by squares in **Fig. 2(b)** and reported in **Fig. 2(a)**. The effect of these irregularities will be brought out in the rest of this paper.

In order to bring out the effect of indenter geometry on the indentation curve, indentation simulations are carried out with the ABAQUS/Standard commercial finite element method code, in axisymmetric mode. Simulations are carried out for both the spherical and the measured non spherical profiles. The mesh composing the indented material sample is made of 10.000 axisymmetric four-node fully integrated elements. The size of the sample and the element density distribution are set in order to obtain a compromise between accuracy in the contact and plastic zones, and computing time, as shown in **Fig. 3**. The lower nodes of the sample are fixed vertically. In section 4, the reverse analysis model proposed by Ogasawara et al. [20] is used, therefore the same conditions are used, i.e. the indenter is supposed rigid, and the maximal vertical displacement of the indenter, or penetration depth, is $h_{max}=75$ μm , i.e. $h_{max}/R=0.3$, for the spherical indenter and, arbitrarily, $h_{max}=100$ μm for the non spherical indenter. Moreover, the Coulomb's friction coefficient is set to 0.15.

Fig. 3. Mesh used for the FEM simulations of indentation (case of the spherical profile)

The indented material obeys isotropic linear elastic behaviour with a Young modulus $E=210$ GPa and a Poisson ratio $\nu=0.3$. The plastic yielding is predicted by the Von Mises yield criterion, the plastic behaviour is isotropic, and the isotropic hardening is described by the Hollomon power law, expressed by Eq. (4).

$$\begin{aligned} \sigma &= E\varepsilon && \text{(Hooke)} && \text{if } \varepsilon < \sigma_y/E \\ \sigma &= E^n \sigma_y^{1-n} \varepsilon^n && \text{(Hollomon)} && \text{if } \varepsilon \geq \sigma_y/E \end{aligned} \quad (4)$$

where σ is the true stress, ε the true strain, σ_y the yield stress and n the hardening coefficient. The twelve σ_y and n value sets are chosen in order to cover a large range of materials, as shown in **Fig. 4**.

Fig. 4. Material parameter values used for the FEM simulations

The indentation curves obtained for each material with the spherical indenter of radius $R'=0.25$ mm and the non spherical indenter are compared in **Fig. 5**.

Fig. 5. Numerical indentation curves obtained with the spherical indenter and the non spherical indenter

The indentation curves obtained with the non spherical indenter are very different from those obtained with the spherical indenter. There is an obvious need for a correction of the curves obtained with the non spherical indenter in order to use reverse analysis models developed for spherical indenters. In section 3, correction methods based on geometrical and physical considerations are proposed and assessed.

3. Correction of the indentation curves obtained with an imperfect spherical indenter

3.1. Definition of the correction methods

In order to correct the indentation curves obtained with an imperfect spherical indenter, two methods (A and B) are assessed. Both methods are based on the calculation of an instantaneous equivalent sphere radius which is used to correct the indentation data. The used geometric values can be either the contact data (subscript c) or the penetration data (no subscript). As shown in **Fig. 6**, both methods provide the instantaneous equivalent sphere radius at equal radii a_c or a for the non spherical indenter and the equivalent sphere. The two methods differ by the second used geometric value. Method A considers the equality of depths h_c or h to calculate the instantaneous sphere radius R_A whereas Method B considers the equality of volumes V_c or V to calculate the instantaneous sphere radius R_B .

Fig. 6. Principles of methods A and B with the use of either the contact data or the penetration data

In the case of the use of the contact data, the equivalent sphere radius R_A is calculated from Eq. (5), which is the same as Eq. (2) used in [22-24].

$$R_A = \frac{a_c^2 + h_c^2}{2h_c} \quad (5)$$

The volume under the contact radius a_c of a sphere of radius R_B is obtained from Eq. (6).

$$V_c = \frac{\pi}{3} \left(R_B - \sqrt{R_B^2 - a_c^2} \right)^2 \left(2R_B + \sqrt{R_B^2 - a_c^2} \right) \quad (6)$$

The analytical inversion of Eq. (6) leads to the expression of the equivalent sphere radius R_B in Eq. (7).

$$R_B = \frac{\pi^{-\frac{1}{3}} X_c^2 + a_c^4 \pi X_c + a_c^8 \pi^{\frac{7}{3}}}{12V_c X_c} \quad (7)$$

where $X_c = \left(648V_c^4 + 72V_c^2 a_c^6 \pi^2 + a_c^{12} \pi^4 + 12V_c \sqrt{(a_c^6 \pi^2 + 9V_c^2)(18V_c^2 + a_c^6 \pi^2)} \right)^{\frac{1}{3}}$

In the case of the use of the penetration data, the same equations are used, after removing the subscript c .

The radii a_c and a are obtained from the discrete definition of the non spherical indenter profile and the volumes V_c and V are obtained from the three-dimensional numerical integration of the profile. The equivalent sphere radii for both methods are plotted versus a_c or a and compared to the reference sphere radius $R'=0.25$ mm in **Fig. 7**.

Fig. 7. Equivalent sphere radii corresponding to methods A and B

For a or a_c values under about 50 μm , R_A shows higher values than R_B . For a or a_c values higher than about 50 μm , R_B shows higher values than R_A . Moreover, the effect of the irregularities of the profile on the equivalent radii is obvious and more pronounced for R_B , as shown by squares in **Fig. 7**.

The availability of an instantaneous equivalent sphere radius allows for an instantaneous dimensionless transformation of the indentation curve. For that purpose, the physical quantity which is considered equal for the spherical and the non spherical indenter is the mean contact pressure, as expressed by Eq. (8) in the case of the use of the contact data.

$$\frac{F'}{\pi a_c'^2} = \frac{F}{\pi a_c^2} \quad (8)$$

where F' and a_c' are the transformed load and contact radius corresponding to the indentation by an ideal spherical indenter of radius R' . In order to fulfil this condition, the load and contact radius are respectively transformed as expressed by Eq. (9) and Eq. (10).

$$F' = \left(\frac{R'}{R_{A \text{ or } B}} \right)^2 F \quad (9)$$

$$a_c' = \frac{R'}{R_{A \text{ or } B}} a_c \quad (10)$$

The transformed contact depth h'_c is obtained from the transformed contact radius a_c from the geometrical relationship applicable to a sphere of radius R' as expressed by Eq. (11).

$$h'_c = R' - \sqrt{R'^2 - a_c'^2} \quad (11)$$

In the case of the use of the penetration data, the same equations are used, after removing the subscript c .

3.2. Use of the penetration data

The contact depth h_c , and consequently the contact radius a_c and the indenter volume V_c under the contact surface, cannot be deduced from the monotonous $F-h$ curve used by reverse analysis models. Indeed, this information would require either the analysis of unloading curves, or the observation of residual imprints [8, 9, 25]. However, the surface contact radius a and the indenter volume V under the initial sample surface can be directly deduced from the known penetration depth h and the profile of the indenter. Therefore, in a first approach, the penetration data, i.e. h , a and V , is used. **Fig. 8** shows the results of corrections A and B using the penetration data.

Fig. 8. Corrections A and B using the penetration data

The result of the corrections is mostly dependant on the hardening coefficient n . The effect of the irregularities of the non spherical indenter profile is mostly observable for $n=0.0$, i.e. apparition of strong pile-up, as brought out by squares. Method A produces poorer results as the n value increases, whereas method B produces good results with the increase of the n value, i.e. in the case of moderate pile-up, no pile-up or sink-in, or sink-in.

3.3. Use of the contact data

Although method B seems to provide adequate results in **Fig. 8**, the dependence on the n value, i.e. the apparition of pile-up or sink-in, suggests that the contact data could be more appropriate for an optimal correction of the indentation curves. Experimentally, the knowledge of the contact data requires more information than the monotonous $F-h$ curve only, i.e. the analysis of unloading curves or the observation of residual imprints. However, in the context of this numerical investigation, the contact data can be obtained from the finite element method code. **Fig. 9** shows the h_c/h ratio versus h for the twelve studied materials, obtained with the spherical indenter and the non spherical indenter.

Fig. 9. Contact depth ratio versus penetration depth

The apparition of pile-up ($h_c/h > 1$) or sink-in ($h_c/h < 1$) is strongly dependant on the n value, and, to a lesser extent, on the E/σ_y value [27]. The h_c/h ratio obtained with the spherical indenter and the non spherical indenter, although quite close, shows noticeable differences. Overall, the non spherical indenter produces a higher h_c/h ratio for low n values and a lower h_c/h ratio for high n values.

The availability of the contact data for both indenters allows for its use in Eq. (5), (7), (9), (10) and (11). For a given penetration depth of the non spherical indenter, the corresponding contact data is used for the transformation. After transformation, the penetration depth of the spherical indenter corresponding to the transformed contact depth is used for the transformed $F'-h'$ curve. **Fig. 10** shows the results of corrections A and B using the contact data.

Fig. 10. Corrections A and B using the contact data

The result of the corrections is mostly dependant on the hardening coefficient n . However, the irregularities of the non spherical indenter profile show no effect on the corrected indentation curves. Method A produces poorer results as the n value increases, as in the case of the use of the penetration data. However, method B produces quality results for all materials, i.e. independently of the n and σ_y values.

These results show that a relevant method to correct the effect of imperfect spherical indenter geometry on the $F-h$ curve is to consider the equality of mean contact pressures obtained with an ideal spherical indenter of radius R' and a spherical indenter whose instantaneous equivalent radius R_{Be} is obtained from the simultaneous equality of contact radii a_c and indenter volumes V_c under the contact surface.

In section 4, a reverse analysis model based on ideal spherical geometry is applied to ideal, initial, and corrected data to confirm the relevance of the proposed correction method.

4. Application of a reverse analysis model

In order to assess the relevance of the proposed correction method, the reverse analysis model proposed by Ogasawara et al. [20] is used. This model is chosen because the simulations were carried out using the same conditions and because the validity of its efficiency and implementation was shown in some of the authors' previous work [26]. The model is applied to MAT 1 ($\sigma_y=200$ MPa, $n=0.0$), MAT 3 ($\sigma_y=200$ MPa, $n=0.2$), MAT 6 ($\sigma_y=600$ MPa, $n=0.1$) and MAT 9 ($\sigma_y=1000$ MPa, $n=0.0$), which are representative of mechanical properties commonly observed for engineering metals. **Table 1** shows the identification results obtained after application of the reverse analysis model on numerical curves obtained with **(a)** the spherical indenter, **(b)** the non spherical indenter assuming a radius $R=0.25$ mm, **(c)** the non spherical indenter after correction B using the penetration data, and **(d)** the non spherical indenter after correction B using the contact data.

(a)

(b)

(c)

(d)

Table 1. Identification results from curves obtained with **(a)** the spherical indenter, **(b)** the non spherical indenter assuming a radius $R=0.25$ mm, **(c)** the non spherical indenter after correction B using the penetration data, and **(d)** the non spherical indenter after correction B using the contact data.

As was shown in some of the authors' previous work [26], the identification results obtained from indentation curves calculated in ideal conditions, i.e. using a spherical indenter, are very close to the input values. However, as can be expected, using the indentation curves obtained with the non spherical indenter and assuming a radius $R=0.25$ mm leads to strongly inaccurate identification results. The use of correction B with the penetration data significantly reduces the identification errors, and the use of correction B with the contact data provides identification results of the same quality than those obtained in ideal conditions. **Fig. 11** shows the corresponding stress-strain curves, which provide a good illustration of the trends described above.

(a) (b)
(c) (d)

Fig. 11. Identified stress-strain curves from curves obtained with (a) the spherical indenter, (b) the non spherical indenter assuming a radius $R=0.25$ mm, (c) the non spherical indenter after correction B using the penetration data, and (d) the non spherical indenter after correction B using the contact data.

The application of a reverse analysis model to the indentation curves calculated in this work confirms the relevance of the proposed correction method.

5. Conclusion

In this paper, the effect of imperfect spherical indenter geometry on the indentation curve was numerically investigated, and correction methods were proposed to transform the indentation curve into one obtained with an ideal spherical indenter, in order to use reverse analysis models developed for spherical indenters. Results showed that a relevant method to correct the effect of imperfect spherical indenter geometry is to consider the equality of mean contact pressures obtained with an ideal spherical indenter and a spherical indenter whose instantaneous equivalent radius is obtained from the simultaneous equality of contact radii and indenter volumes under the contact surface. The application of a reverse analysis model on the indentation curves confirmed the necessity of a correction method and the efficiency of the proposed method.

In conclusion, with the knowledge of the real indenter geometry and the contact radius, reverse analysis models based on ideal spherical indenter geometry can be efficiently applied on indentation curves obtained with an imperfect indenter using the proposed method. This is of particular interest in the case of low scale indenters for which perfect indenter geometry is difficult to achieve. In future work, the effect of indenter deformation and the determination of the contact radius will be investigated.

References

- [1] Doerner M.F., Nix W.D. A method for interpreting the data from depth-sensing indentation instruments. *J. Mater. Res.* 1, 601 (1986).
- [2] Oliver W.C., Pharr G.M. An improved technique for determining hardness and elastic modulus using load and displacement sensing indentation experiments. *J. Mater. Res.* 7, 1564 (1992).
- [3] Loubet JL, Georges JM, Meille G. Vickers indentation curves of elastoplastic materials. *Microindentation techniques in materials science and engineering. ASTM STP 889* (1986).
- [4] International Standard ISO 14577-1:2002. Metallic materials – Instrumented indentation test for hardness and materials parameters – Part 1: Test method.
- [5] International Standard ISO 14577-2:2002. Metallic materials – Instrumented indentation test for hardness and materials parameters – Part 2: Verification and calibration of testing machines.
- [6] International Standard ISO 14577-3:2002. Metallic materials – Instrumented indentation test for hardness and materials parameters – Part 3: Part 3: Calibration of reference blocks.
- [7] International Standard ISO 14577-4:2002. Metallic materials – Instrumented indentation test for hardness and materials parameters – Part 4: Test method for metallic and non-metallic coatings.
- [8] Ahn J-H, Kwon D. Derivation of plastic stress–strain relationship from ball indentations: Examination of strain definition and pileup effect. *J. Mater. Res.*, Vol. 16, No. 11, Nov 2001.
- [9] Kim J-Y, Lee K-W, Lee J-S, Kwon D. Determination of tensile properties by instrumented indentation technique: Representative stress and strain approach. *Surface & Coatings Technology* 201 (2006) 4278–4283.

- [10] Kucharski S, Mröz Z. Identification of plastic hardening parameters of metals from spherical indentation tests. *Mater Sci Eng A* 2001;318:65.
- [11] Nayebi A, El Abdi R, Bartier O, Mauvoisin G. New procedure to determine steel mechanical parameters from the spherical indentation technique. *Mech Mater* 2002;34:243.
- [12] Cao Y-P, Lu J. A new method to extract the plastic properties of metal materials from an instrumented spherical indentation loading curve. *Acta Mater* 2004;52:4023.
- [13] Lee H, Lee JH, Pharr GM. A numerical approach to spherical indentation techniques for material property evaluation. *J Mech Phys Solids* 2005;53:2037.
- [14] Beghini M, Bertini L, Fontanari V. Evaluation of the stress–strain curve of metallic materials by spherical indentation. *Int J Solids Struct* 2006;43:2441.
- [15] Zhao M, Ogasawara N, Chiba N, Chen X-A. A new approach to measure the elasticplastic properties of bulk materials using spherical indentation. *Acta Mater* 2006;54:23.
- [16] Cao Y, Qian X, Huber N. Spherical indentation into elastoplastic materials: indentation-response based definitions of the representative strain. *Mat Sci Eng A* 2007;454:1.
- [17] Collin J-M, Mauvoisin G, Bartier O, El Abdi R, Pilvin P. Experimental evaluation of the stress–strain curve by continuous indentation using different indenter shapes. *Mat Sci Eng A* 2009;501:140.
- [18] Collin J-M, Mauvoisin G, Pilvin P. Materials characterization by instrumented indentation using two different approaches. *Mater Des* 2010;31:636.
- [19] Jiang P, Zhang T-H, Feng Y-H, Liang N-G. Determination of plastic properties by instrumented spherical indentation: expanding cavity model and similarity solution approach. *J Mater Res* 2009;24:1045.
- [20] Ogasawara N, Chiba N, Chen X. A simple framework of spherical indentation for measuring elastoplastic properties. *Mech Mater* 2009;41:1025.

[21] Lee JH, Kim T, Lee H. A study on robust indentation techniques to evaluate elastic-plastic properties of metals. *Int J Solids Struct* 2010;47:647.

[22] Constantinides G, Silva ECCM, Blackman GS, Van Vliet KJ. Dealing with imperfection: quantifying potential length scale artefacts from nominally spherical indenter probes. *Nanotechnology* 18 (2007) 305503 (14pp).

[23] Kang S-K, Kim Y-C, Kang I, Kwon D. Effective indenter radius and frame compliance in instrumented indentation testing using a spherical indenter. *J. Mater. Res.*, Vol. 24, No. 9, Sep 2009.

[24] Kang S-K, Kim Y-C, Lee Y-H, Kim J-Y, Kwon D. Determining effective radius and frame compliance in spherical nanoindentation. *Materials Science and Engineering A* 538 (2012) 58–62.

[25] Collin J-M, Mauvoisin G, El Abdi R. An experimental method to determine the contact radius changes during a spherical instrumented indentation. *Mechanics of Materials* 40 (2008) 401–406.

[26] Brammer P, Bartier O, Hernot X, Mauvoisin G, Sablin S-S. An alternative to the determination of the effective zero point in instrumented indentation: use of the slope of the indentation curve at indentation load values. *Materials and Design* 40 (2012) 356-363.

[27] Hernot X, Bartier O, Bekouche Y, El Abdi R, Mauvoisin G. Influence of penetration depth and mechanical properties on contact radius determination for spherical indentation. *International Journal of Solids and Structures* 43 (2006) 4136–4153.

Fig. 1.

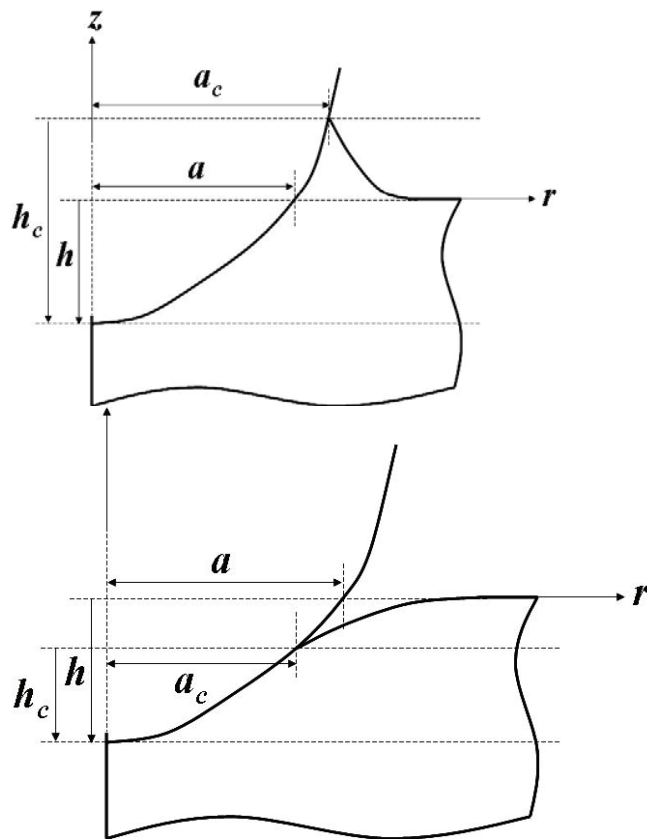


Fig. 2.

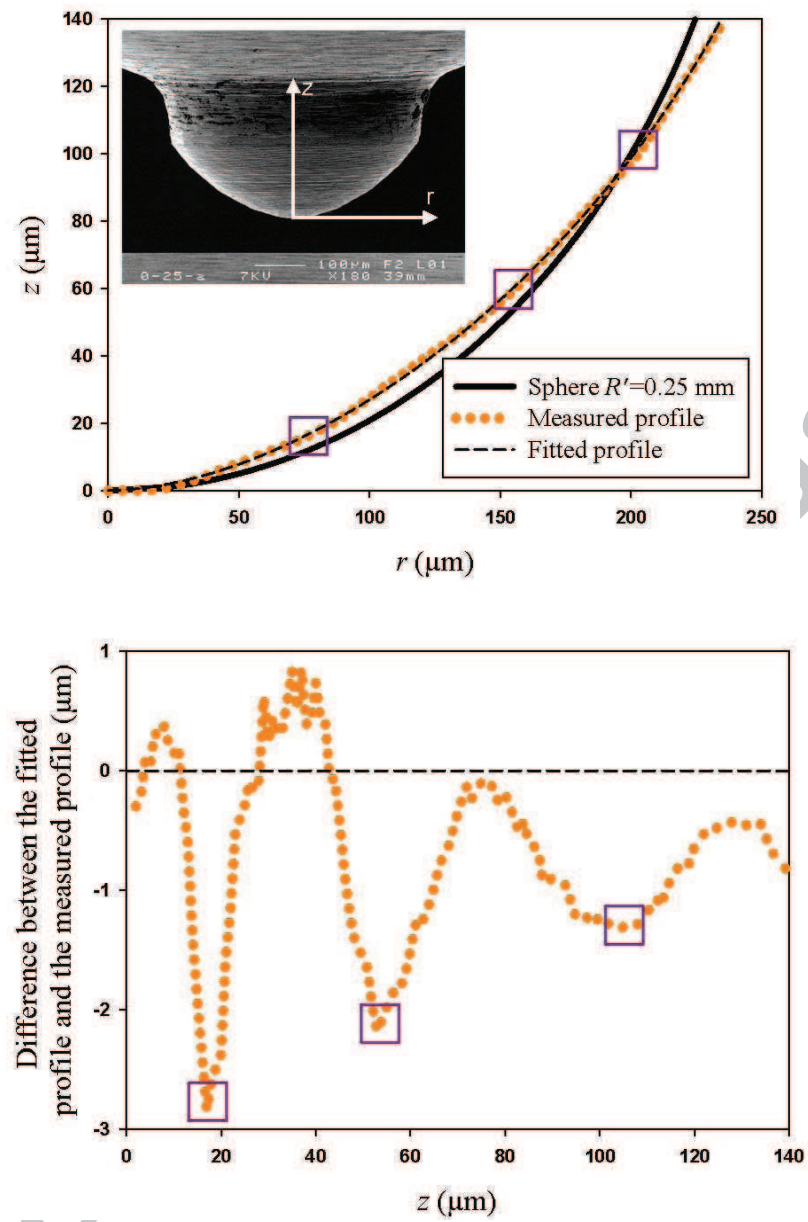
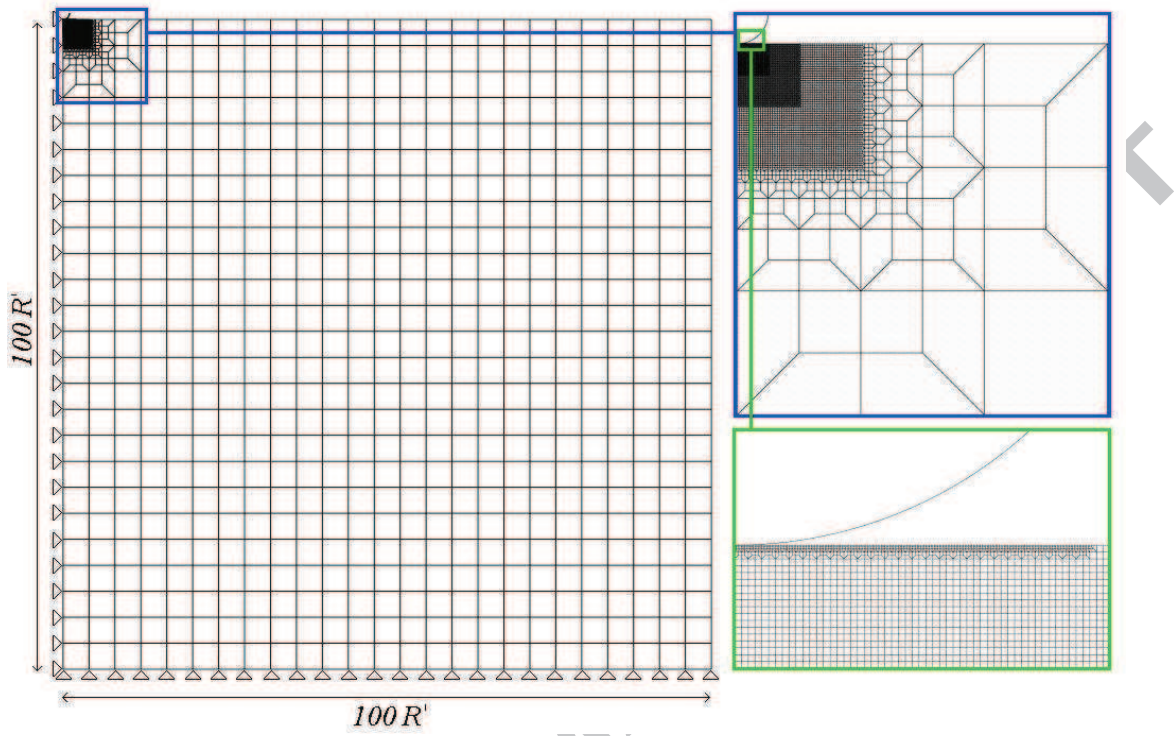


Fig. 3.



ACCEPTED MANUSCRIPT

Fig. 4.

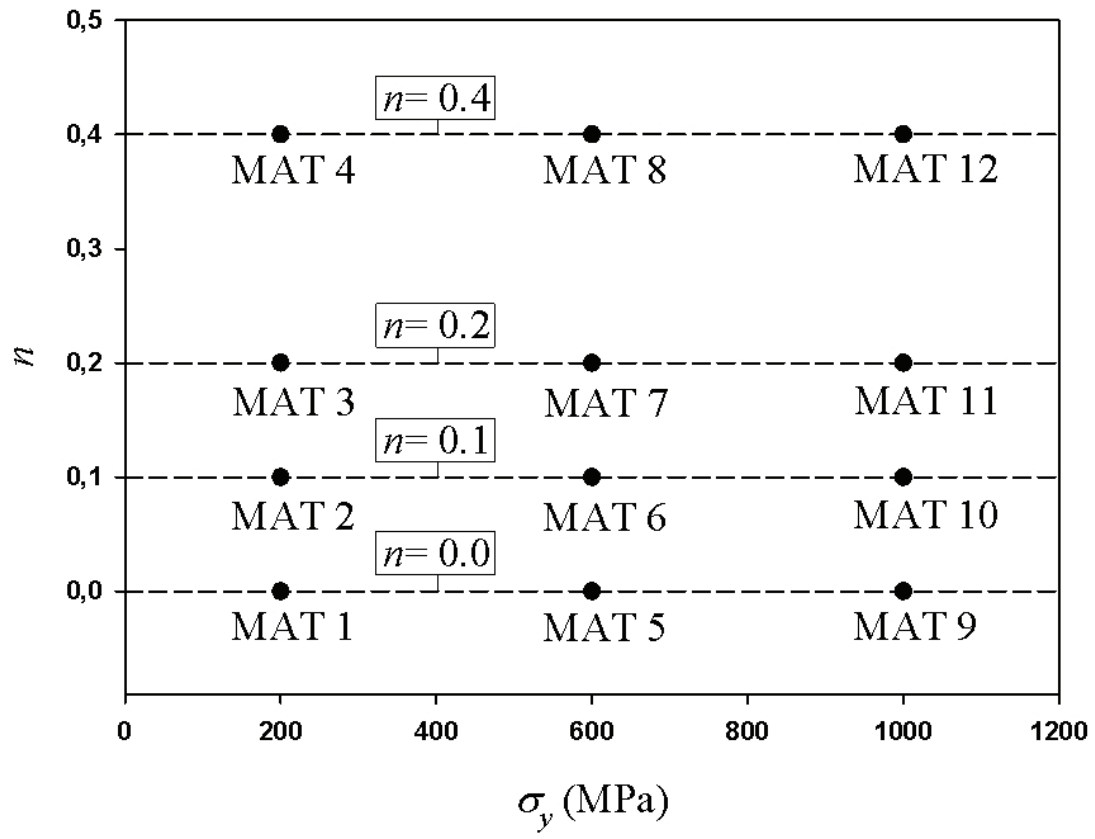


Fig. 5.

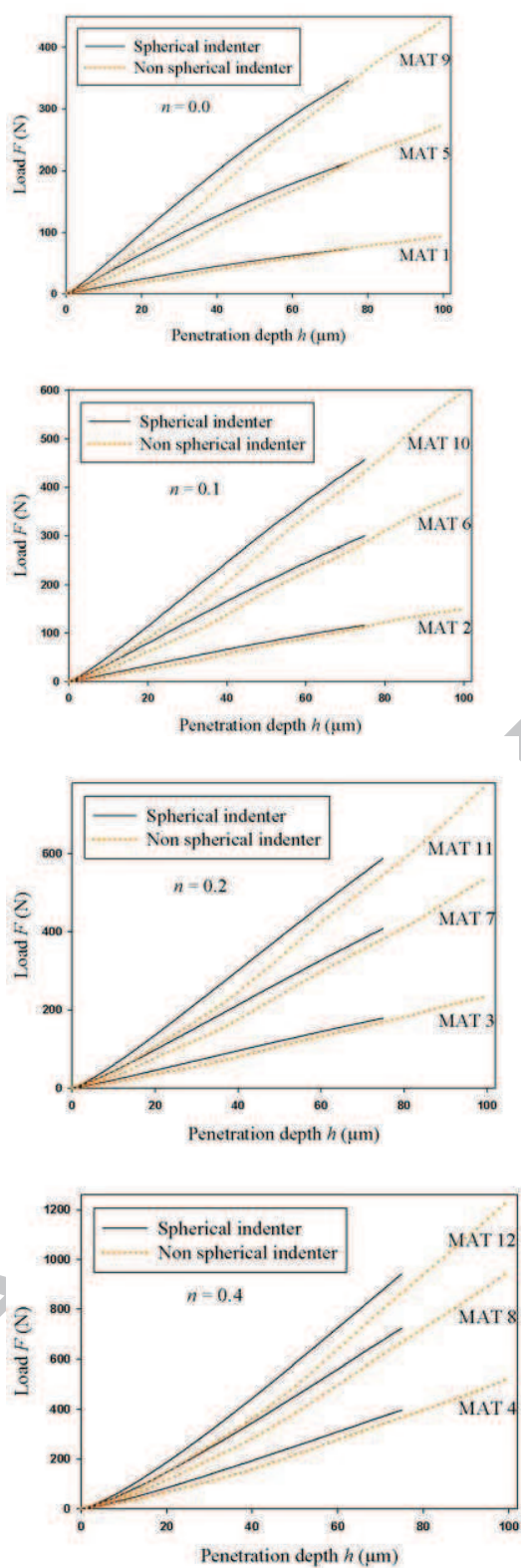


Fig. 6.

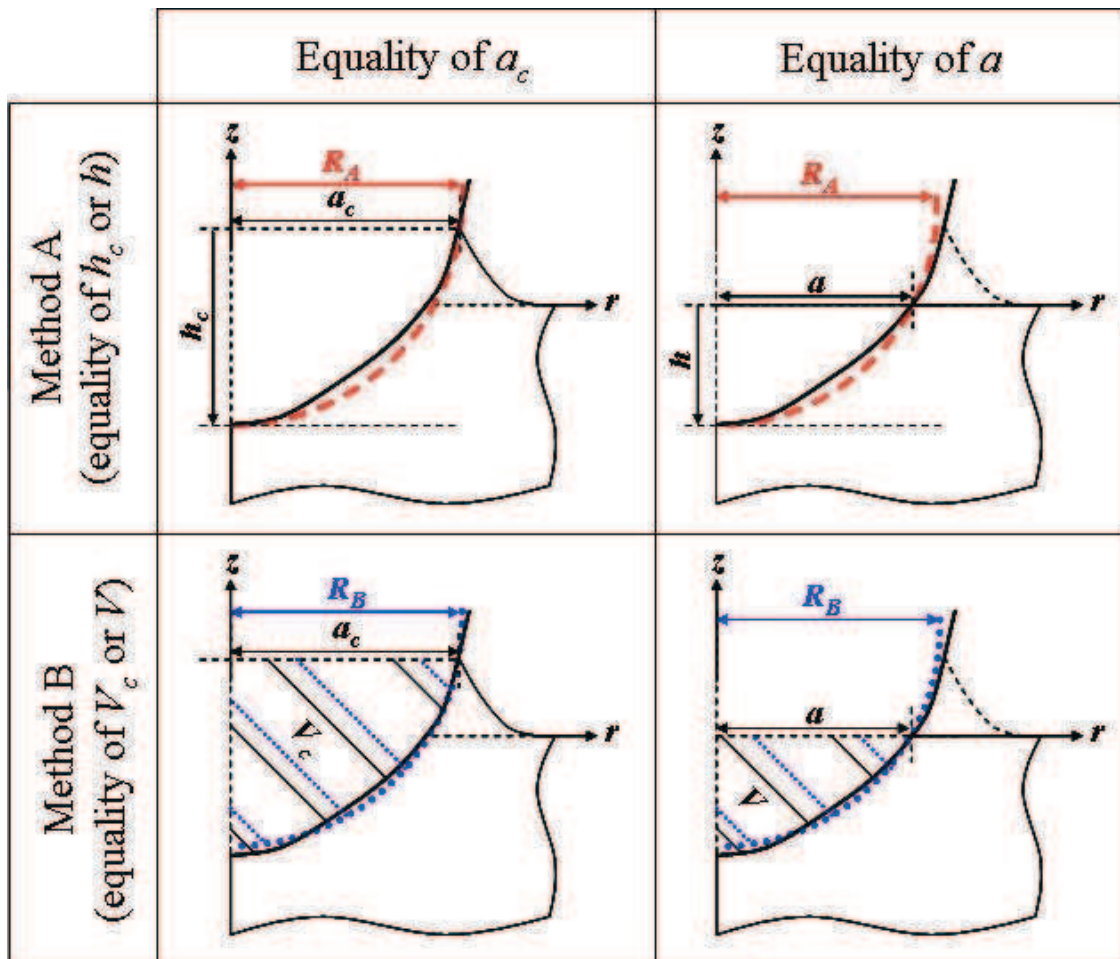
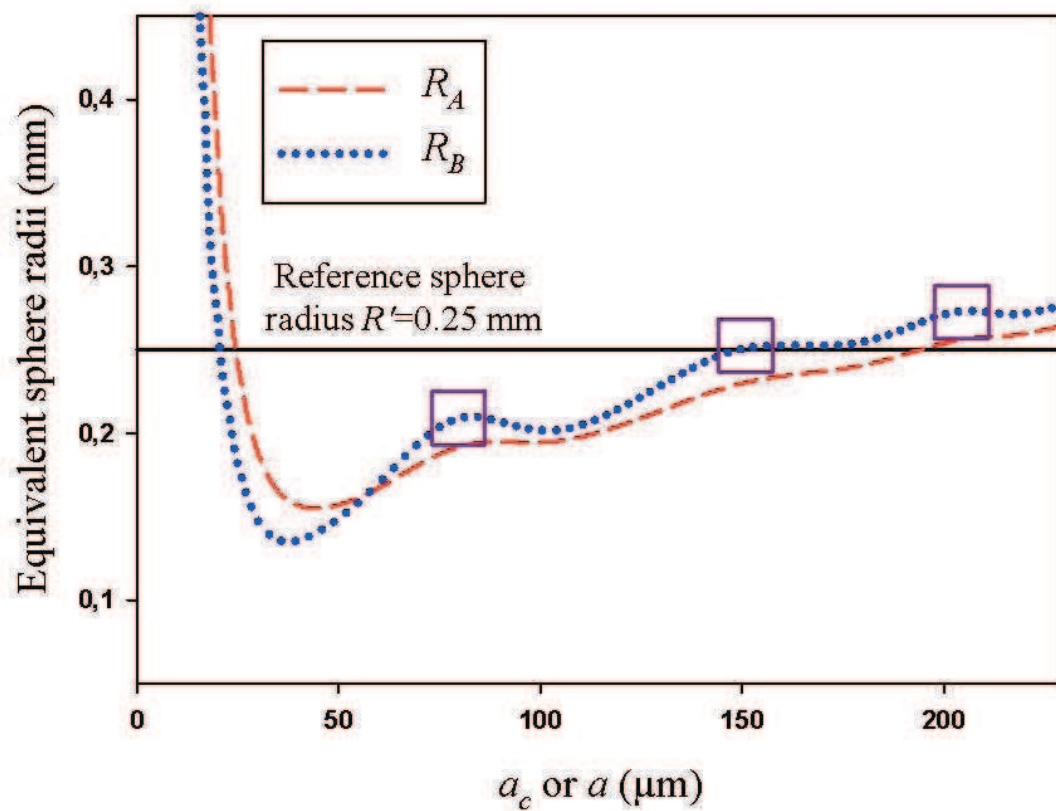


Fig. 7.



ACCEPTED

Fig. 8.

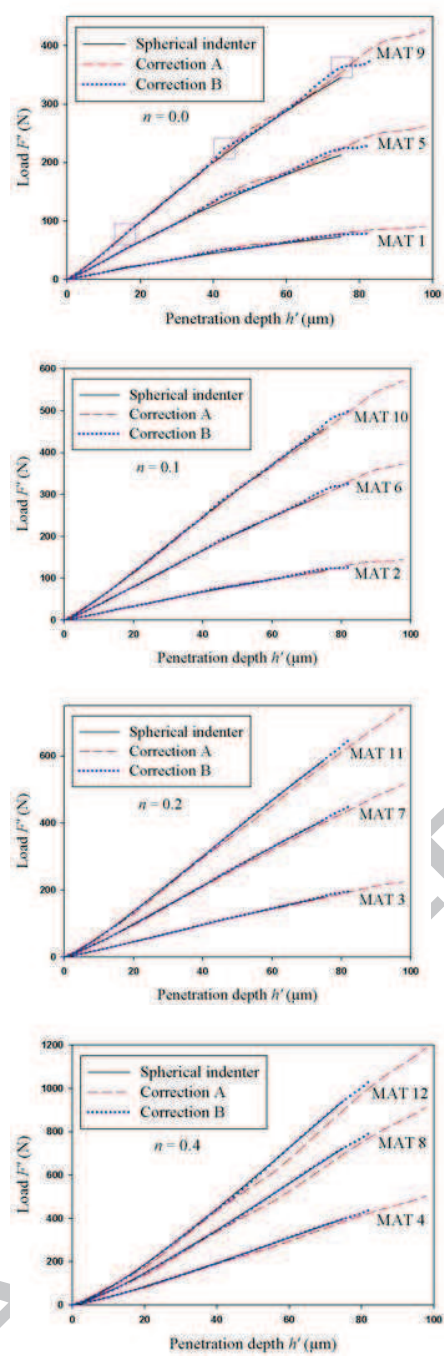


Fig. 9.

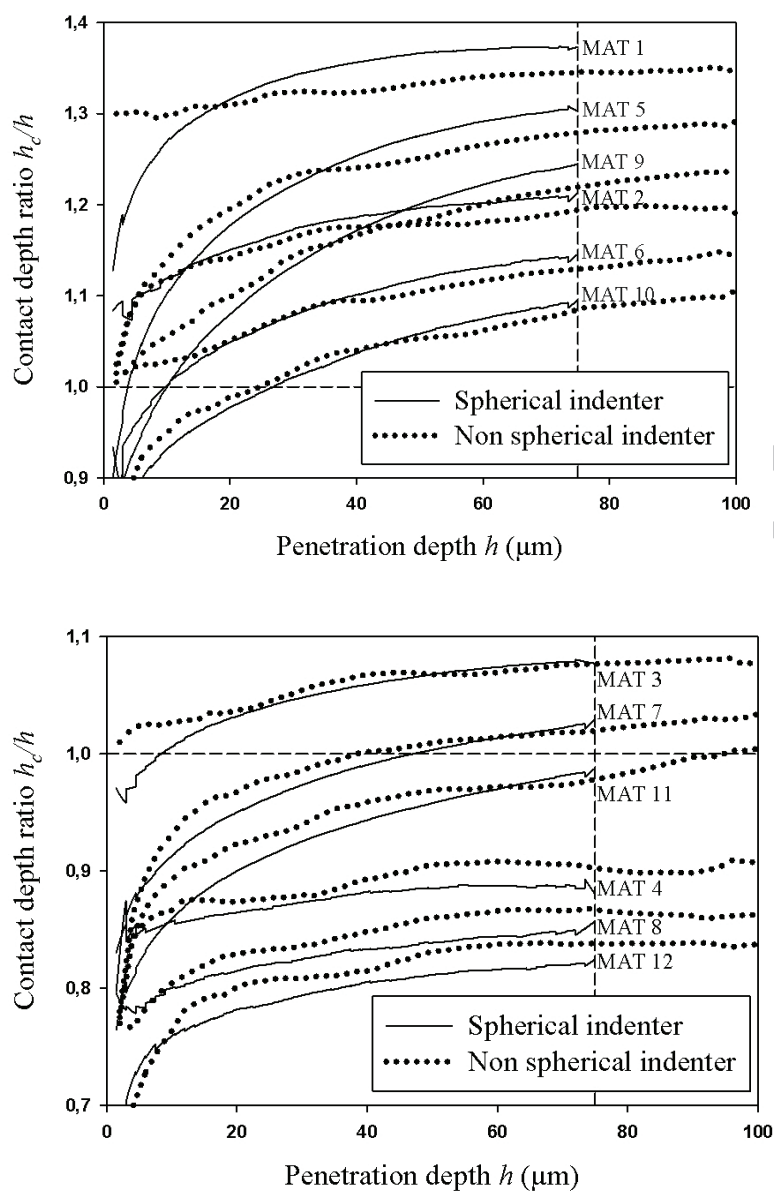


Fig. 10.

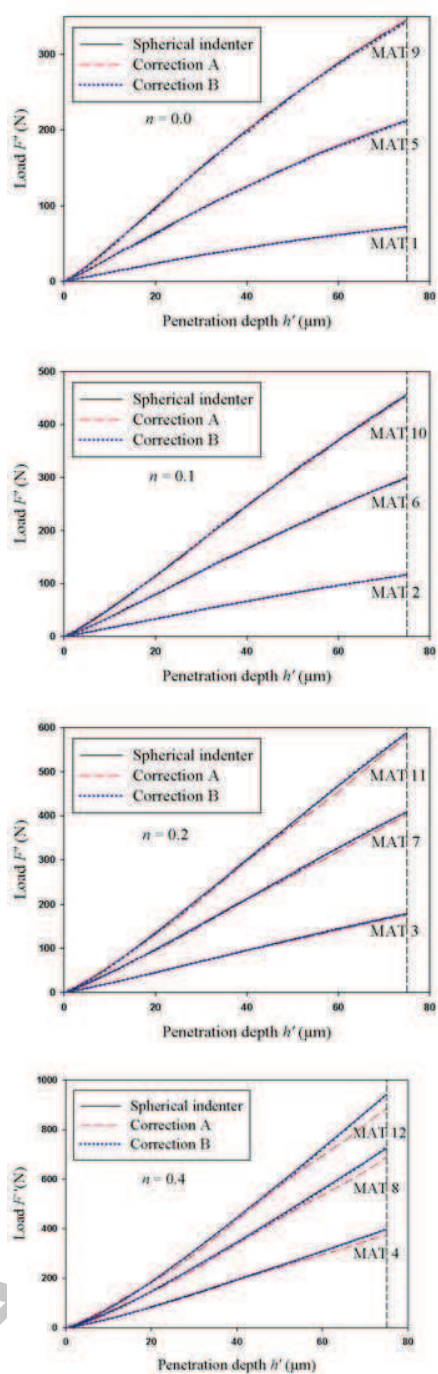
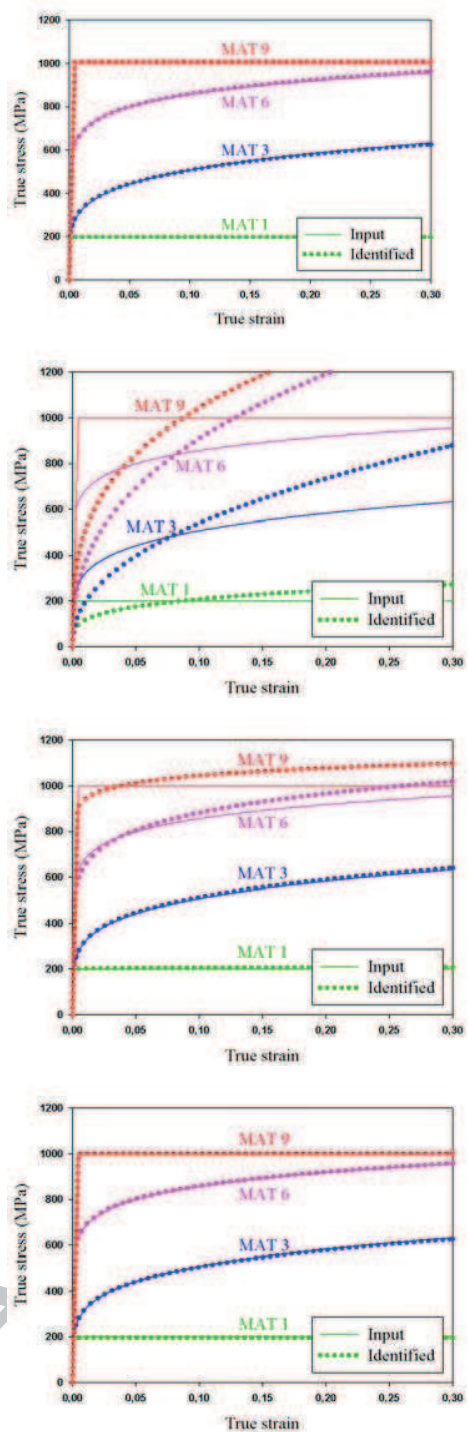


Fig. 11.



Spherical indenter				
	σ , (MPa)	Error (%)	n	Error (%)
MAT 1	197	-1.5	0.000	/
MAT 3	209	+4.5	0.192	-4.0
MAT 6	593	-1.2	0.104	+4.0
MAT 9	1009	+0.9	0.000	/

Non spherical indenter				
	σ , (MPa)	Error (%)	n	Error (%)
MAT 1	45	-77.5	0.249	/
MAT 3	29	-85.5	0.444	+122.0
MAT 6	121	-79.8	0.391	+291.0
MAT 9	261	-73.9	0.316	/

Correction B. penetration data				
	σ , (MPa)	Error (%)	n	Error (%)
MAT 1	197	-1.5	0.01	/
MAT 3	202	+1.0	0.201	+0.5
MAT 6	547	-8.8	0.131	+31.0
MAT 9	907	-9.3	0.045	/

Correction B. contact data				
	σ , (MPa)	Error (%)	n	Error (%)
MAT 1	196	-2.0	0.000	/
MAT 3	205	+2.5	0.195	-2.5
MAT 6	605	+0.8	0.099	-1.0
MAT 9	1001	+0.1	0.000	/

Highlights

The effect of imperfect spherical indenter geometry on indentation load-depth curves is brought out.

An efficient method to correct indentation curves is proposed.

A reverse analysis model is applied using the corrected curves, leading to an accurate identification of elastoplastic properties.

ACCEPTED MANUSCRIPT